

IV. CONCLUSION

In this study, myocardial strain rate was measured at high temporal resolution, realizing the frame rate of 630 Hz. From *in vivo* experimental results, it was found that properties of the myocardial contraction/relaxation varies, depending on the depth in the heart wall, and there is a delay from one side to another side in each heart wall at the beginning of contraction and relaxation. At the same time, from two-dimensional movies of strain rate, it was recognized that the timing of contraction and relaxation was different between the apex and base side. These results show a potential of this method for estimation of the physiological function of myocardium.

REFERENCES

- [1] G. R. Sutherland, G. D. Salvo, P. Claus, J. D'hooge, and B. Bijnens, "Strain and strain rate imaging: a new approach to quantifying regional myocardial function," *J. Am. Soc. Echocardiogr.*, vol. 17, no. 7, pp. 788-802, 2004.
- [2] H. Kanai, M. Sato, Y. Koiwa, and N. Chubachi, "Transcutaneous measurement and spectrum analysis of heart wall vibrations," *IEEE Trans. Ultrason., Ferroelect., Freq. Contr.*, vol. 43, no. 5, pp. 791-810, 1996.
- [3] H. Kanai, H. Hasegawa, N. Chubachi, Y. Koiwa, and M. Tanaka, "Noninvasive evaluation of local myocardial thickening and its color-coded imaging," *IEEE Trans. Ultrason., Ferroelect., Freq. Contr.*, vol. 44, no. 4, pp. 752-768, 1997.
- [4] J. D'hooge, E. Konofagou, F. Jamal, A. Heimdal, L. Barrios, B. Bijnens, J. Thoen, F. V. Werf, G. Sutherland, and P. Suetens, "Two-dimensional ultrasonic strain rate measurement of the human heart *in vivo*," *IEEE Trans. Ultrason., Ferroelect., Freq. Contr.*, vol. 49, no. 2, pp. 281-286, 2000.

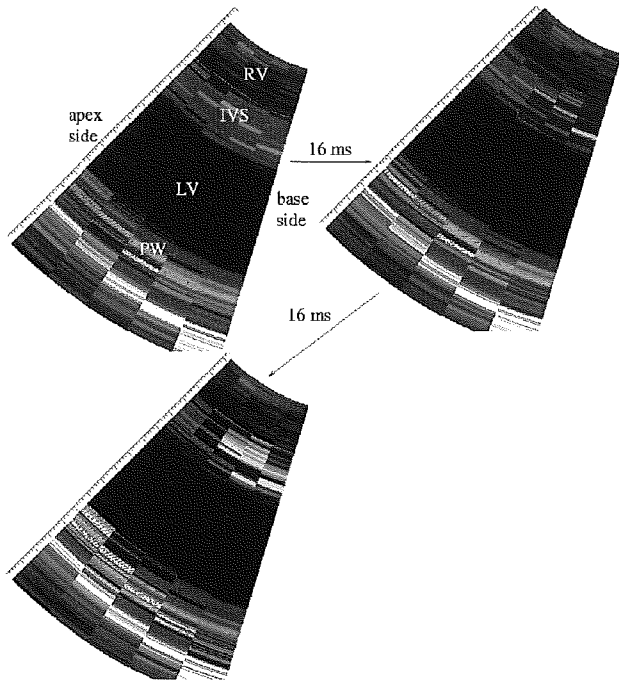


Figure 5: Two-dimensional distribution of strain rate around the second heart sound.

Development of Speed-of-Sound Microscopy for Biomedical Applications

Y. Saijo, H. Sasaki, E. Santos Filho, T. Yambe, M. Tanaka
Department of Medical Engineering and Cardiology
Institute of Development, Aging and Cancer, Tohoku University
4-1 Seiryomachi, Aoba-ku, Sendai 980-8575, Japan
saijo@idac.tohoku.ac.jp

N. Hozumi
Department of Electrical and Electronic Engineering
Graduate School, Toyohashi University of Technology
1-1 Tempaku, Toyohashi, 441-8580, Japan

K. Kobayashi, N. Okada
Research & Development Headquarters
Honda Electronics Co. Ltd.
20 Oyamazuka, Oiwa-cho, Toyohashi, 441-3193, Japan

Abstract— We have been developing a scanning acoustic microscope (SAM) system for medicine and biology featuring quantitative measurement of ultrasonic speed and attenuation of soft tissues. In the present study, we will propose a new concept ultrasonic speed microscopy that can measure the thickness and ultrasonic speed using fast Fourier transform of a single pulsed wave instead of continuous waves used in conventional SAM systems. Six coronary arteries were frozen and sectioned approximately 10 μ m in thickness. They were mounted on glass slides without cover slips. The scanning time of a frame with 300 \times 300 pixels was 30 s and two-dimensional distribution of ultrasonic speed was obtained. The ultrasonic speed was 1720 m/s in the thickened intima with collagen fiber, 1520 m/s in lipid deposition underlying fibrous cap and 1830m/s in calcified lesion in the intima. These basic measurements will help understanding echogenicity in intravascular ultrasound (IVUS) images. Imaging of coronary artery with the ultrasonic speed microscopy provides important information for study of IVUS coronary imaging.

Keywords; *acoustic microscopy, ultrasonic speed, coronary artery, atherosclerosis*

I. INTRODUCTION

Since 1985, we have been developing a scanning acoustic microscope (SAM) system for biomedical use and have been investigating the acoustic properties of various organs and disease states by using this SAM system [1-9]. In biomedicine, SAM is useful for intraoperative pathological examination, study of low-frequency ultrasonic images, and assessment of biomechanics at a microscopic level. The most important feature of our SAM system lies in providing quantitative

values of ultrasonic speed and attenuation of thin slices of soft tissue.

In the present study, we will propose a new concept ultrasonic speed microscopy that can measure the thickness and ultrasonic speed using fast Fourier transform of a single pulsed wave instead of continuous waves used in conventional SAM systems. We measured the ultrasonic speed of the tissue components in coronary arteries and the results were compared with IVUS imaging of coronary artery in clinical settings.

II. METHODS

A. Tissue Preparation

Six human coronary artery specimens were involved in the present study. At the autopsy, the coronary arteries were frozen with OCT compounds, sectioned approximately 10 μ m in thickness to make a cross-sectional view of coronary artery and mounted on glass slides. The specimens were not stained or not covered with cover slips for ultrasonic speed microscopy observation.

B. Speed-of-Sound Microscopy

Fig. 1 shows a block diagram of speed of sound microscopy for biological tissue characterization. A single ultrasound pulse with a pulse width of 6 ns was emitted and received by the same transducer above the specimen. The aperture diameter of the transducer was 1.2 mm, and the focal length was 1.5 mm. The central frequency was 80 MHz, the bandwidth was 40-150 MHz, and the pulse repetition rate was 10 kHz. The diameter of the focal spot was estimated to be 20 μ m at 80 MHz by taking into account the focal distance and

sectional area of the transducer. Distilled water was used as the coupling medium between the transducer and the specimen. The reflections from the tissue surface and those from the interface between the tissue and glass were received by the transducer and were introduced into a Windows-based PC (Pentium 4, 2.8 GHz, 1GB RAM, 80GB HDD) via an analogue-digital converter (Acqiris DP-210, Switzerland). The frequency range was 500 MHz, and the sampling rate was 2 GS/s. Eight values of the time taken for a pulse response at the same point were averaged in order to reduce random noise.

The transducer was mounted on an X-Y stage with a microcomputer board that was driven by the PC through RS232C. The Both X-scan and Y-scan were driven by linear servo motors. Finally, two-dimensional distributions of ultrasonic intensity, speed of sound, attenuation coefficient and thickness of a specimen measuring 2.4×2.4 mm were visualized using 300×300 pixels. The total scanning time was 90 s.

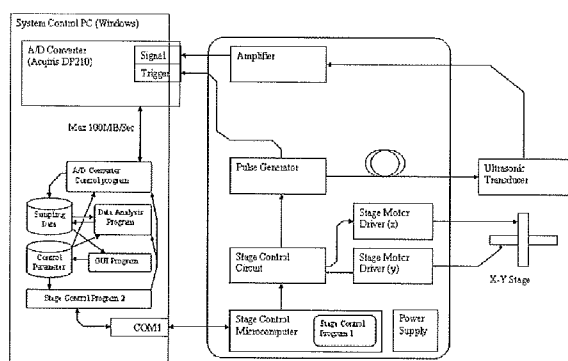


Figure 1. Block diagram of ultrasonic speed microscopy developed with collaboration between Tohoku University, Toyohashi University of Technology and Honda Electronics Co. Ltd.

Fig. 2 shows the appearance of the speed-of-sound microscopy. Whole system can be placed on the desktop.

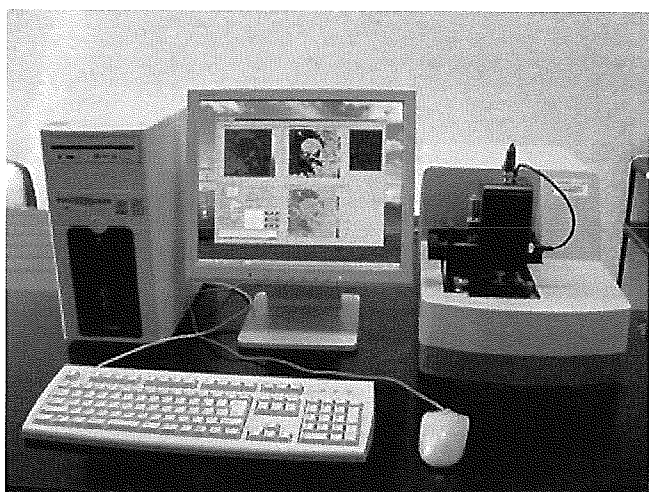


Figure 2. Appearance of this speed-of-sound microscopy.

C. Signal Analysis [10]

The reflected waveforms are shown in Fig. 3. The waveform at the glass surface without the tissue is shown in (a). This signal was used as a reference waveform. The decline of the glass surface was compensated by measuring three different points in the glass area surrounding the tissue. The waveform from the tissue area is shown in (b). Although the waveform contains two reflections at the surface and at the interface of the tissue and glass, the two components cannot be separated in time domain analysis. Thus, frequency domain analysis was performed by analyzing the interference between the two reflections. Intensity and phase spectra were calculated by Fourier transforming the waveform. The spectra were normalized by the reference waveform. Fig. 4 shows the frequency domain analysis of the interfered waveform.

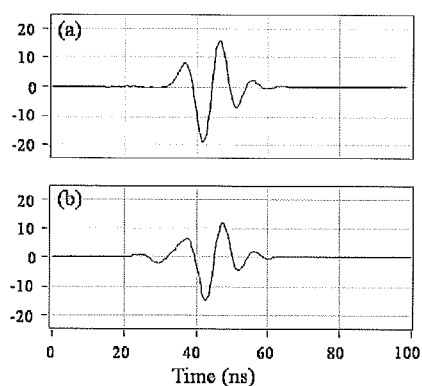


Figure 3. Reflected waveforms (a) from the glass surface without tissue, and (b) from the tissue area

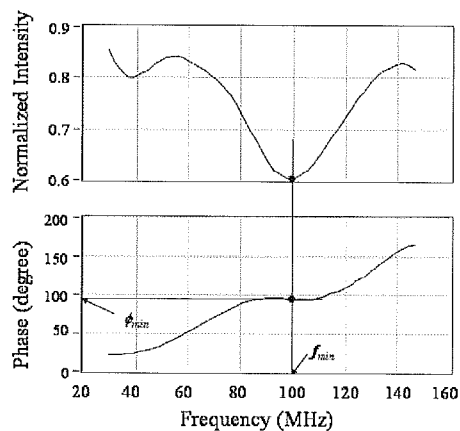


Figure 4. Frequency domain analysis of interfered waveform. f_{min} : the minimum point in the intensity spectrum, ϕ_{min} : corresponding phase angle

Denoting the minimum point in the intensity spectrum by f_{min} and the corresponding phase angle by ϕ_{min} , the phase difference between the two reflections at the minimum point is $(2n-1)\pi$, which yields

$$2\pi f_{min} \times \frac{2d}{c_0} = \phi_{min} + (2n-1)\pi \quad (1)$$

where d , c_0 , and n are the tissue thickness, sound speed of water, and a non-negative integer, respectively. Denoting the maximum point in the intensity spectrum by f_{max} and the corresponding phase angle by ϕ_{max} , the phase difference at the maximum point is $2n\pi$, which yields

$$2\pi f_{max} \times \frac{2d}{c_0} = \phi_{max} + 2n\pi \quad (2)$$

The phase angles ϕ_{min} and ϕ_{max} can be expressed by

$$2\pi f_{min} \times 2d \left(\frac{1}{c_0} - \frac{1}{c} \right) = \phi_{min} \quad (3)$$

$$2\pi f_{max} \times 2d \left(\frac{1}{c_0} - \frac{1}{c} \right) = \phi_{max} \quad (4)$$

since ϕ_{min} or ϕ_{max} is the phase difference between the wave that travels the distance $2d$ with sound speed c and the wave that travels a corresponding distance with sound speed c_0 . By solving equations (1) and (3),

$$d = \frac{c_0}{4\pi f_{min}} \{ \phi_{min} + (2n-1)\pi \} \quad (5)$$

is obtained for the minimum point. Solving equations (2) and (4) yields

$$d = \frac{c_0}{4\pi f_{max}} (\phi_{max} + 2n\pi) \quad (6)$$

for the maximum point. Finally, the sound velocity at each frequency is calculated as

$$c = \left(\frac{1}{c_0} - \frac{\phi_{min}}{4\pi f_{min} d} \right) \quad (7)$$

$$c = \left(\frac{1}{c_0} - \frac{\phi_{max}}{4\pi f_{max} d} \right) \quad (8)$$

After determination of the thickness, attenuation of ultrasound was then calculated by dividing amplitude by the thickness.

III. RESULTS

Fig. 5 shows a PC window of our speed-of-sound microscopy. The upper left is an amplitude image, the upper right is an ultrasonic speed image, the lower left is an attenuation image and the lower right is the thickness

distribution of the normal coronary artery. The intima is thin and speed of sound is 1600 m/s in the intima, 1560 m/s in the media and 1590 m/s in the adventitia, respectively.

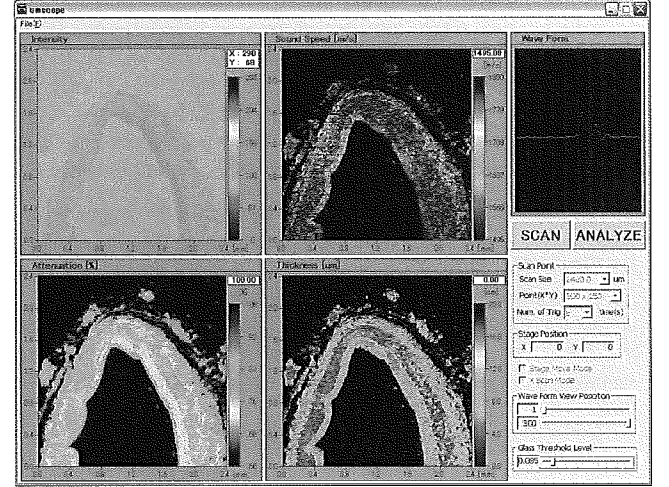


Figure 5. PC window of speed of sound microscopy showing a normal coronary artery. Upper left: amplitude image, upper right: speed of sound image, lower left: attenuation image and lower right: thickness

Fig. 6 is an atherosclerotic coronary artery. The speed of sound is 1680 m/s in the thickened intima with collagen fiber, 1520 m/s in lipid deposition underlying fibrous cap and 1810m/s in calcified lesion in the intima.

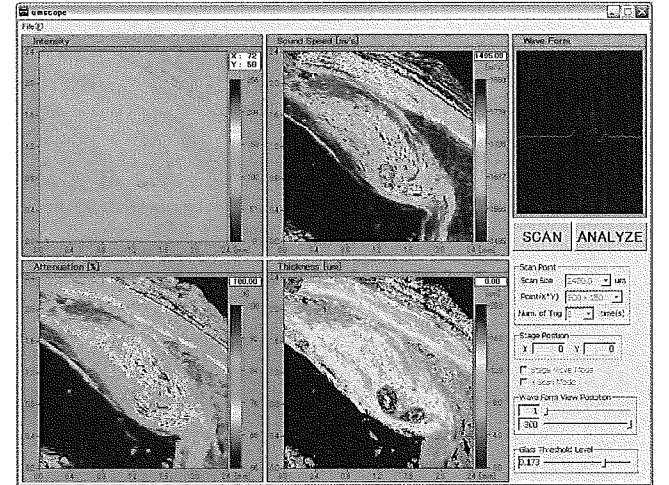


Figure 6. PC window of speed of sound microscopy showing an atherosclerotic coronary artery. Upper left: amplitude image, upper right: speed of sound image, lower left: attenuation image and lower right: thickness.

IV. DISCUSSION

In the present study, speed of sound in the excised human coronary arteries was measured with the ultrasonic speed microscopy. The results would become basic data base for interpretation of clinical IVUS images and novel IVUS imaging technologies.

The results showed that the speed of sound in the intima and adventitia, mainly consisted of collagen fiber, had higher values than those of media, mainly consisted of vascular smooth muscle. The different of acoustic properties may lead to the classical three-layered appearance of normal coronary artery in clinical IVUS imaging. The findings indicate that the echo intensity is not determined by the difference of acoustic impedance between neighboring layers. The distribution and the structure of materials with different acoustic properties may also contribute to the echo pattern in IVUS.

The plaque with a thick fibrous cap consisted of collagen fiber, considered showed higher value of speed of sound than those of normal media. Generally, absorption and scattering are the two main factors of attenuation of ultrasound. Thus, the high scattering within the thickened intima may lead to the high intensity echo in the "hard plaque". Lipid showed speed of sound. These values explain the low echo in the "soft plaque" in the same manner of renal cysts containing water like fluid. Besides its absolute low values, the homogeneity of acoustic properties within the lipid pool may contribute to the low scattering and consequently a lipid pool shows low intensity echo.

V. CONCLUSIONS

We have developed a novel acoustic microscope system that can measure the speed of sound of thin slices of biological material. The most important feature was use of a single pulse and the Fourier transform to calculate the sound speed at all measuring points. Although the data acquisition time of a frame was greater than that in conventional SAM, the total time required for calculation was significantly shorter. The acoustic microscope system can be applied to intraoperative pathological examination.

ACKNOWLEDGMENTS

This study was supported by Grants-in-Aid for Scientific Research (Scientific Research (B) 15300178, Scientific Research (B) 15360217) from the Japan Society for the Promotion of Science and Health and Labor Sciences Research Grants from the Ministry of Health, Labor and Welfare for the Research on Advanced Medical Technology (H17-Nano-001).

REFERENCES

- [1] Y. Saijo, M. Tanaka, H. Okawai, F. Dunn, The ultrasonic properties of gastric cancer tissues obtained with a scanning acoustic microscope system, *Ultrasound Med Biol* 17 (1991), pp. 709-714.
- [2] H. Sasaki, M. Tanaka, Y. Saijo, H. Okawai, Y. Terasawa, S. Nitta, K. Suzuki, Ultrasonic tissue characterization of renal cell carcinoma tissue, *Nephron* 74 (1996), pp. 125-130.
- [3] Y. Saijo, M. Tanaka, H. Okawai, H. Sasaki, S. Nitta, F. Dunn, Ultrasonic tissue characterization of infarcted myocardium by scanning acoustic microscopy, *Ultrasound Med Biol* 23 (1997), pp. 77-85.
- [4] Y. Saijo, H. Sasaki, H. Okawai, S. Nitta, M. Tanaka, Acoustic properties of atherosclerosis of human aorta obtained with high-frequency ultrasound, *Ultrasound Med Biol* 24 (1998), pp. 1061-1064.

- [5] Y. Saijo, H. Sasaki, M. Sato, S. Nitta, M. Tanaka, Visualization of human umbilical vein endothelial cells by acoustic microscopy, *Ultrasonics* 38 (2000), pp. 396-399.
- [6] Y. Saijo, T. Ohashi, H. Sasaki, M. Sato, C.S. Jorgensen, S. Nitta, Application of scanning acoustic microscopy for assessing stress distribution in atherosclerotic plaque, *Ann Biomed Eng* 29 (2001), pp. 1048-53.
- [7] H. Sasaki, Y. Saijo, M. Tanaka, S. Nitta, Influence of tissue preparation on the acoustic properties of tissue sections at high frequencies, *Ultrasound Med Biol* 29 (2003), pp. 1367-72.
- [8] Y. Saijo, T. Miyakawa, H. Sasaki, M. Tanaka, S. Nitta, Acoustic properties of aortic aneurysm obtained with scanning acoustic microscopy, *Ultrasonics* 42 (2004), pp. 695-698.
- [9] H. Sano, Y. Saijo, S. Kokubun, Material properties of the supraspinatus tendon at its insertion – A measurement with the scanning acoustic microscopy, *J. Musculoskeletal Res.* 8 (2004), pp. 29-34.
- [10] N. Hozumi, R. Yamashita, C.K. Lee, M. Nagao, K. Kobayashi, Y. Saijo, M. Tanaka, N. Tanaka, S. Ohtsuki, Time-frequency analysis for pulse driven ultrasonic microscopy for biological tissue characterization, *Ultrasonics* 42 (2004), pp. 717-722.

Imaging for Biological Tissue with Acoustic Impedance Microscope

A.Kimura, S. Terauchi, Y. Murakami,
N. Hozumi, M. Nagao, S. Yoshida
Toyoashi University of Technology
Toyoashi, Japan
kimura@boss.eee.tut.ac.jp

K. Kobayashi

Honda Electronics Co., Ltd
Toyoashi, Japan

Y. Saijo

Tohoku University
Sendai, Japan

Abstract—We have proposed a new method for two-dimension for two-dimensional acoustic impedance imaging for biological tissue that can perform micro-scale observation without preparing a sliced specimen. A tissue was attached on a substrate of 0.5mm in thickness. An acoustic pulse was transmitted from the "rear side" of the substrate. The reflection intensity was interpreted into local acoustic impedance of the target tissue. Quantification of acoustic impedance was performed using water or an appropriate material as a reference. As for an observation, rat cerebellum was employed. The development of parallel fiber in cerebella cultures was clearly observed as the contrast in acoustic impedance. The proposed technique is believed to be a powerful tool for biological tissue characterization.

Keywords-component; biological tissue; acoustic impedance; micro-scale imaging

I. INTRODUCTION

In most of optical observation of biological tissue, the specimen is sliced into several micrometers in thickness, and fixed on a glass substrate. The microscopy is obtained by transmitted light through the specimen. As it is normally not easy to get a good contrast by local difference in refraction and/or transmission spectrum, the specimen is usually stained before being observed. However the staining has some disadvantages. It normally takes from several hours to several days to finish the process. Furthermore, the tissue, after being stained, often completely loses its biological functions; i.e., the observation with staining process is chemically destructive.

The authors previously proposed a pulse driven ultrasonic sound speed microscopy that can obtain sound speed image in a short time [1-2]. Although a small roughness of the specimen was approved in this type of microscope, slicing the specimen into several micrometers was still required for the observation.

Based on the above background, the authors newly propose the acoustic impedance microscopy that can image the local distribution of cross sectional acoustic impedance of tissue. As acoustic impedance is given as a product of sound speed and density, it would have a good correlation with sound speed, when the variance in density was not significant

II. EXPERIMENTAL SETUP

Fig. 1 illustrates the outline of the acoustic impedance microscope. Distilled water was used for the coupling medium between the substrate and transducer. A sharp electric pulse of about 40 V in peak voltage and 2 ns in width was generated by

the pulse generator. The maximum repetition rate of the pulse was as high as 10 kHz. The transducer was PVDF-TrFE type of which focal length was 3.0 mm. An acoustic wave with a wide frequency component was generated by applying the voltage pulse. The acoustic wave, being focused on the interface between the substrate and tissue, was transmitted and received by the same transducer. Two-dimensional profile of acoustic impedance was obtained by mechanically scanning the transducer using the stage driver, keeping the focal point on the rear surface of the substrate.

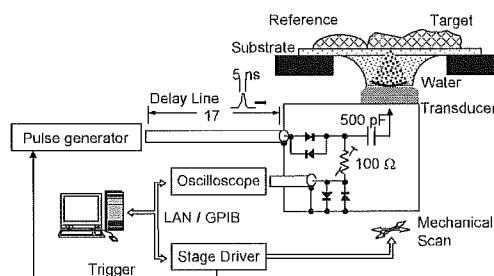


Fig. 1 Overview of a part of the experiment system.

III. CALIBRATION

Figure 2 illustrates the calibration of acoustic impedance. The target signal is compared with the reference signal. Hereafter, the signal component at an arbitrary frequency will be symbolized by S . Considering the reflection coefficient, the target signal S_{target} can be described as

$$S_{\text{target}} = \frac{Z_{\text{target}} - Z_{\text{sub}}}{Z_{\text{target}} + Z_{\text{sub}}} S_0$$

where S_0 is the transmitted signal, Z_{target} and Z_{sub} are the acoustic impedances of the target and substrate, respectively. On the other hand, the reference signal can be described as

$$S_{\text{ref}} = \frac{Z_{\text{ref}} - Z_{\text{sub}}}{Z_{\text{ref}} + Z_{\text{sub}}} S_0$$

where Z_{ref} is the acoustic impedance of the reference material. We can measure S_{target} and Z_{ref} , however, S_0 can not be directly measured. The acoustic impedance of the target is

subsequently calculated as a solution of the simultaneous equations for Z_{target} and S_0 , as

$$Z_{target} = \frac{1 - \frac{S_{target}}{S_0}}{1 + \frac{S_{target}}{S_0}} Z_{sub} = \frac{1 - \frac{S_{target}}{S_{ref}} \cdot \frac{Z_{sub} - Z_{ref}}{Z_{sub} + Z_{ref}}}{1 + \frac{S_{target}}{S_{ref}} \cdot \frac{Z_{sub} - Z_{ref}}{Z_{sub} + Z_{ref}}} Z_{sub}$$

assuming that S_0 is constant throughout the observation process.

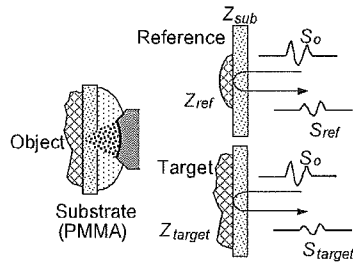


Fig.2 Illustration for calibration of the acoustic impedance.

IV. OBSERVATION OF CEREBELLAR CORTEX OF A RAT

Figure. 3 shows the observed images of cerebellar cortex of a rat at immature (P1; postnatal 1 day), transient (P7), and mature (P20) stages. All the specimens in Fig. 3 had been chemically fixed.

In the immature cerebellar cortex (P1), the external granular layer (EGL), the outer layer of the cortex, showed higher impedance compared to the inner layer. The area indicated by the rectangle in the acoustic image is morphologically corresponding to the immunohistochemical observation, although the scale is not completely corresponded because the tissue was somehow subjected to compression during the acoustic observation. At this stage, as myelin is not yet generated, the existence of white matter (WM) is not clearly observed.

In the medium stage, four different layers; the WM, internal granular layer (IGL), Purkinje layer (PL) and EGL become to be comprehensive. The EGL and IGL showed higher impedance than the PL and WM. Morphological correspondence between acoustic and immunohistological observation is however not clear in these images.

In the mature stage, the EGL, which is composed of small neuronal cell bodies, has developed into the molecular layer (ML), which is composed of elongated axon (neurite), called parallel fibers. The four layers, WM, IGL, PL and ML are more clearly observed in acoustic image. The correspondence with immunohistological observation is also clearly seen.

It should be noted that very similar image were observed by simply contacting a cross section of the whole tissue with the substrate, without performing chemical fixation.

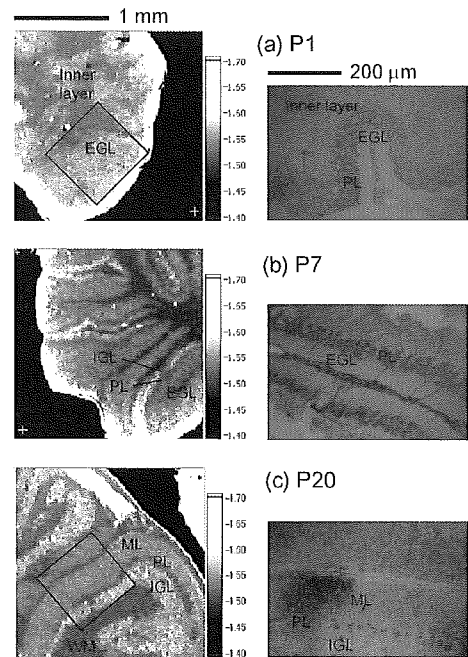


Fig.3 Two-dimensional profiles of acoustic impedance ($\times 10^6 \text{Ns/m}^3$) of cerebellar cortex (left) and optical microcopies (right). Specimen: rat, sagittal cross section, chemically fixed.

V. DISCUSSION

Considering the precision of the calibration, the reference material should be stable in both physical and chemical properties, and should strongly adhere to the substrate. It is recommended that the acoustic impedance of the reference is close to that of the target. Furthermore, as for the substrate, most of available materials have higher acoustic impedance than biological tissues. In such cases, the phase of the transmitted signal is reversed at the interface. The acoustic impedance of the substrate should be sufficiently high compared to that of the target, in order to retain a strong reflection. However extremely high acoustic impedance of the substrate may increase the reflection coefficient at the interface between the coupling medium and substrate, and reduce the intensity of transmitted signal to the target. This would obviously reduce the S/N ratio. Therefore, in order to obtain a good S/N ratio, the materials should be carefully selected considering their accordance.

REFERENCES

- [1] N. Hozumi, R. Yamashita, C-K Lee, M. Nagao, K. Kobayashi, Y. Saijo, M. Tanaka, N. Tanaka & S. Ohtsuki: "Ultrasonic Sound Speed Microscope for Biological Tissue Characterization Driven by Nanosecond Pulse", *Acoustic Science & Technology*, **20**, 386 (2003).
- [2] N. Hozumi, R. Yamashita, C-K. Lee, M. Nagao, K. Kobayashi, Y. Saijo, M. Tanaka, N. Tanaka & S. Ohtsuki: "Time-frequency analysis for pulse driven ultrasonic microscopy for biological tissue characterization", *Ultrasonics*, **42**, 717 (2003).

Increased Sound Speed of Synovial Membrane after Immobilization Assessed by Scanning Acoustic Microscopy

Yoshihiro Hagiwara^{1*}, Yoshifumi Saijo², Fujio Matsumoto¹, Eiichi Chimoto¹, Yasuyuki Sasano³,
Shoichi Kokubun¹

¹Department of Orthopaedic Surgery, Tohoku University Graduate School of Medicine, ²Department of Medical Engineering and Cardiology, Institute of Development, Aging and Cancer, Tohoku University, ³Division of Craniofacial Development and Regeneration, Tohoku University Graduate School of Dentistry

Sendai, Japan

hagi@mail.tains.tohoku.ac.jp

Abstract

Objectives: The biomechanics of immobilized joints is not well understood. The present study was designed to investigate the tissue elasticity of the anterior and posterior synovial membrane (SM) in a rat immobilized knee model using scanning acoustic microscopy (SAM).

Methods: Thirty rats had their knee joints immobilized with a plate and metal screws. The rats were fixed at 1, 2, 4, 8 and 16 weeks after surgery and the knee joints were sectioned sagittally. A new concept SAM using a single pulsed wave instead of continuous waves was applied to measure the sound speed of the anterior and posterior SM, comparing it with the corresponding light microscopic images.

Results: The sound speed of the posterior SM increased significantly in the 8- and 16-week experimental group compared with that in the control group. The sound speed of the anterior SM showed no statistical difference between the experimental and the control groups at any period of immobilization.

Conclusions: Our data suggest that the increased elasticity of the posterior SM after a long period of immobilization in flexion is one of the main causes of limited extension. SAM is a powerful tool for evaluating the elasticity of targeted tissues.

Keywords-immobilization, knee, contracture, scanning acoustic microscopy, elasticity, synovial membrane

I. INTRODUCTION

Joint contracture is defined as a decrease in both active and passive ranges of motion (ROM) after immobilization. The decreased ROM limits the activity of daily living in various aspects. Immobilization, which is a major cause of joint contracture, is beneficial for decreasing pain caused by trauma and preventing the joint from damage in the acute phase of arthritis such as pyogenic and rheumatoid arthritis (1-3). Even by extensive rehabilitation or surgical treatment, however, it is difficult to regain the full ROM in an established joint contracture after a long period of immobilization (4,5).

The components of joint contracture after immobilization are classified into arthrogenic and myogenic ones. The arthrogenic components are lesions of bone, ligaments, capsule and synovial membrane (SM), while the myogenic components

are lesions of muscle, tendon and fascia (6,7). Some investigators have attributed contracture to myogenic causes (8), while others attributed it to arthrogenic causes (4,7,9-13). It is difficult to evaluate such contradictory reports because different animal species and methods were used in their immobilization experiments. Among the arthrogenic components, the stiffness of the capsule and SM through synovial atrophy, retraction, fibrosis, and adhesion may contribute to the limited ROM (1,7,8,10,14-17). Though increased elasticity of the capsule or SM has been suggested to be a cause of joint contracture (18), it is not known yet how the elasticity is affected by immobilization.

A conventional scanning acoustic microscopy (SAM) using continuous waves characterizes biological tissues by determining the elastic parameters based on the sound speed (19). Recent studies on infarcted myocardium (20), atherosclerosis of aorta (21) and carotid arterial plaques (22) have shown that the acoustic properties reflect the collagen types. Though this traditional system still works today, it is not practical because it takes much time to analyze the data.

In the present study, we applied a new concept SAM using single pulsed wave, which can make total time for calculation significantly shorter, to examine the elasticity of the anterior and posterior SM (synovial intima and subintima) in the course of knee joint immobilization in a rat experimental model.

II. MATERIALS AND METHODS

Animals

The protocol for this experiment was approved by the Animal Research Committee of Tohoku University. Adult male Sprague-Dawley rats weighing from 380 to 400 g were used. Their knee joints were immobilized at 145° in flexion with a plastic plate and metal screws for various periods (1, 2, 4, 8 and 16 weeks) (3). The knee joint capsule and the joint itself were untouched (Figure 1A). Sham operated animals had holes drilled in the femur and tibia and screws inserted but none of them were plated. The immobilized animals and the

sham operated animals made up the experimental groups and the control groups, respectively (n=3/ each group).

Tissue Preparation

The rats were fixed with 4% paraformaldehyde in 0.1M phosphate-buffer by perfusion through the aorta. The knee joints were resected and kept in the same fixative. The fixed specimens were decalcified in 10% EDTA in 0.01M phosphate-buffer. The embedded tissue was cut into 5- μ m thick sagittal sections from the medial to the lateral side of the joint. Standardized serial sections of the medial midcondylar region of the knee were made. The serial sections were prepared for hematoxylin-eosin to observe the histological appearance of SM after immobilization.

Scanning acoustic microscopy

Our SAM consists of five parts: 1) ultrasonic transducer, 2) pulse generator, 3) digital oscilloscope with PC, 4) microcomputer board and 5) display unit (Figure 2). A single pulsed ultrasound with 5 ns pulse width was emitted and received by the same transducer above the specimen. The aperture diameter of the transducer was 1.2 mm and the focal length was 1.5 mm. The central frequency was 80 MHz and the pulse repetition rate was 10 kHz. Considering the focal distance and the sectional area of the transducer, the diameter of the focal spot was estimated as 20 μ m at 80 MHz. Distilled water was used as the coupling medium between the transducer and the specimen. The reflections from the tissue surface and from interface between the tissue and the glass were received by the transducer and were introduced into a digital oscilloscope (Tektronics TDS 5052, USA). The frequency range was 300 MHz and the sampling rate was 2.5 GS/s. Four pulse responses at the same point were averaged in the oscilloscope in order to reduce random noise.

The transducer was mounted on an X-Y stage with a microcomputer board that was driven by the computer installed in the digital oscilloscope through an RS-232C. The X-scan was driven by a linear servo-motor and the Y-scan was driven by a stepping motor. Finally, two-dimensional distributions of the ultrasonic intensity, sound speed and thickness of the 2.4 by 2.4 mm specimen area were visualized with 300 by 300 pixels. The total scanning time was 121 sec.

Signal Analysis

The reflected waveform comprises two reflections at the surface and the interface between the tissue and the glass. The thickness and sound speed were calculated by Fourier-transforming the waveform (19).

Image analysis

Normal light microscopic images corresponding to the stored acoustic images were captured (DMLB 100 HC light microscope, LEICA Wetzlar, Germany). A region of analysis by SAM was set in the anterior and posterior SM each in each section (Figure 1B). In the region, the sound speed of SM, excluding meniscus, bone and cartilage, was calculated with a gray scale SAM images using commercially available image analysis software (PhotoShop 6.0, Adobe Systems Inc., San Jose, CA). SAM images with a gradation color scale were also produced for clear visualization of the sound speed. The

optical and acoustic images were compared to ensure morphological congruence in the analysis.

Statistics

All data were expressed as the mean \pm SD. The statistical significance of difference in the results was evaluated by unpaired analysis of variance, and *P* values were calculated by Tukey's method. A *P* value less than 0.05 was considered statistically significant.

III. RESULTS

The gradation color images of the posterior SM in the experimental group differed from that in the control group (Figure 3). The posterior SM was composed of low sound speed area (black to blue) in 2-week immobilization (Figure 3A). Low sound speed area was decreased and high sound speed area (yellow to red) gradually increased in the posterior SM of the experimental group with time (Figure 3B). The posterior SM was remained same in all the control groups (Figure 3C).

The anterior SM was similar in all the experimental and control groups irrespective of immobilization periods (data not shown).

The sound speed of the posterior SM is shown in Figure 4. There was no statistical difference between the experimental and the control groups in 1-, 2- or 4-week immobilization. In 8- and 16-week immobilization, however, the sound speed in the experimental group was significantly higher than that in the control group (8w: 1565 m/s \pm 7.61 m/s vs 1639 m/s \pm 6.02 m/s; *p*<0.005, 16w: 1551 m/s \pm 12.5 m/s vs 1650 m/s \pm 9.18 m/s; *p*<0.005) (Figure 4A). There was no statistical difference in the anterior SM in all the experimental and the control groups at any period of immobilization (Figure 4B).

IV. DISCUSSION

The arthrogenic component has been considered as an important factor of joint contracture after immobilization (1,7,8,10,14-18). In a study using a rabbit knee contracture model, the biomechanical characteristics were quantified by a torque-angular displacement diagram (18). The knees in 9-week immobilization in flexion showed a significantly larger torque in extension in the experimental groups than in the control groups even after total extra-articular myotomies. In the same rat model as ours in the present study but immobilized up to 32-week, ROM in extension remained still restricted even after total extra-articular myotomies, which suggested the myogenic restriction proportionally decreased over time (7). In canine glenohumeral joint immobilized up to 16 weeks, the intra-articular pressure rose higher by injection of Hypaque contrast medium and the filling volume was smaller comparing with the control group at a rupture of the capsule (23). These studies suggest that among the arthrogenic components, the capsule and SM may most contribute to making joint contracture.

Previous studies analyzed the elasticity of the joint as a whole with or without muscles including ligament, capsule and SM (7,15,18,23). But it was impossible to evaluate the elasticity of the individual arthrogenic components, especially

of capsule and SM in those studies. The present study is the first that measured the elasticity of SM in situ by SAM in rat immobilized knees and revealed the increased elasticity of SM as one of the main causes of joint contracture.

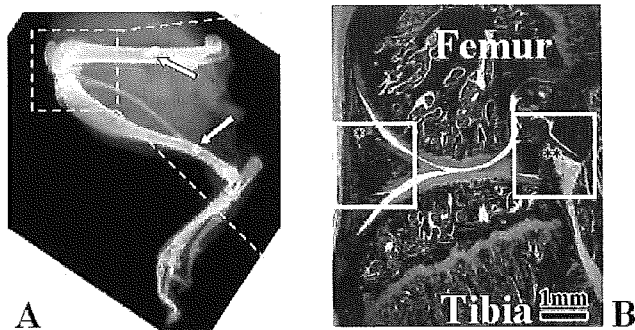


Figure 1: Method of joint immobilization and microrphotograph of a sagittal section in the medial midcondylar region of a rat knee. .
A. Lateral radiograph of the experimental group with a radiolucent plate (20v, 2.0mA, 10sec). Arrows indicate metal screws. **B.** Squares indicate the region of analysis by scanning acoustic microscopy in the anterior (*) and posterior (***) synovial membrane. (Original magnification $\times 10$, hematoxylin-eosin stain)

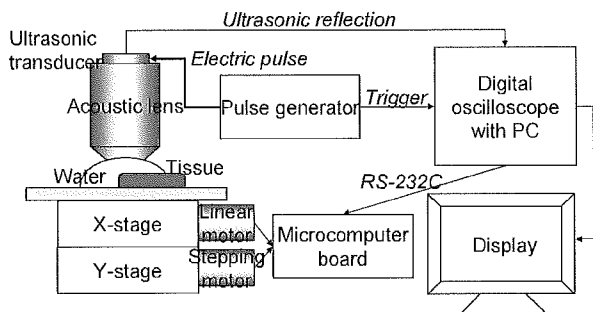


Figure 2: Schematic illustration of a new concept scanning acoustic microscopy.

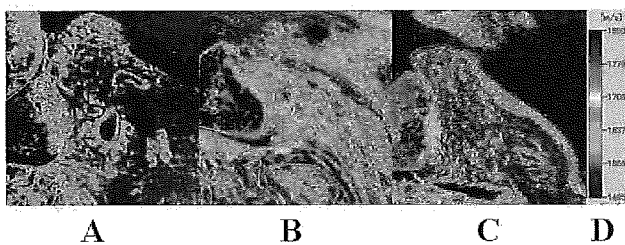


Figure 3: Gradation color images of scanning acoustic microscopy.
A. 2-week immobilization group. **B.** 16-week. **C.** a representative of the control groups (16-week). **D.** gradation color table.

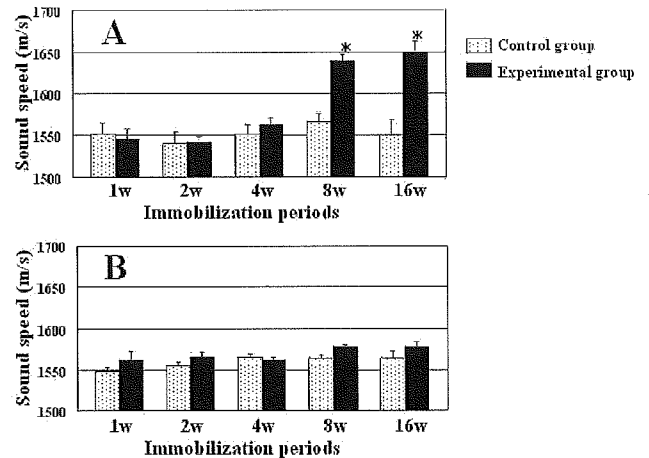


Figure 4: Sound speed changes of the synovial membrane (SM). **A.** the posterior SM. **B.** the anterior SM. In the posterior SM, significant difference of sound speed is seen in 8- and 16-week immobilization. There was no statistical difference at any period of immobilization in the anterior SM. * = $P < 0.005$.

Acknowledgment

The authors would like to acknowledge their valued input and efforts of Mr. Katsuyoshi Shoji, Mrs. Michiko Fukuyama and Miss Haruka Sasaki and thank Dr. Hans K Uhtoff and Dr. Guy Trudel for their technical advice of making the animal model.

REFERENCES

- [1] Trudel G, Seki M, Uhtoff HK. Synovial adhesions are more important than pannus proliferation in the pathogenesis of knee joint contracture after immobilization: an experimental investigation in the rat. *J Rheumatol*, vol27, pp. 351-357, 2000.
- [2] Patridge REH, Duthie JJR. Controlled trial of the effect of complete immobilization of the joints in rheumatoid arthritis. *Ann Rheum Dis*, vol 22, pp.91-99, 1963.
- [3] Gault SJ, Spyker JM. Beneficial effect of immobilization of joints in rheumatoid and related arthritis: A splint study using sequential analysis. *Arthritis Rheum*, vol 12, pp. 34-44, 1969.
- [4] Peacock EE. Some biochemical and biophysical aspects of joint stiffness: role of collagen synthesis as opposed to altered molecular bonding. *Ann Surg*, vol 64, pp.1-12, 1966.
- [5] Damron TA, Greenwald TA, Breed A. Chronological outcome of surgical tendoachilles lengthing and natural history of gastro-soleus contracture in cerebral palsy. *Clin Orthop*, vol 301, pp. 249-255, 1994.
- [6] Trudel G.. Differentiating the myogenic and arthrogenic components of joint contractures. An experimental study on the rat knee joint. *Int J Rehabil Res*, vol 20, pp. 397-404, 1997.
- [7] Trudel G, Uhtoff HK. Contractures secondary to immobility: is the restriction articular or muscular? An experimental longitudinal study in the rat knee. *Arch Phys Med Rehabil*, vol 81, pp. 6-13, 2000.
- [8] Evans BE, Eggers GWN, Butler JK, Blumel J. Experimental immobilization and remobilization of rat knee joints. *J Bone Joint Surg*, vol 42A, pp. 737-758 1960.
- [9] Amiel D, Akeson WH, Harwood FL, Mechanic GL. The effect of immobilization on the types of collagen synthesized in periparticular connective tissue. *Connect Tissue Res*, vol 8, pp. 27-32, 1980.
- [10] Enneking WF, Horowitz M. The Intra-articular effects of immobilization on the human knee. *J Bone Joint Surg*, vol 54A, pp. 973-985, 1972.
- [11] Hall MC. Cartilage changes after experimental immobilization of the knee joint of the young rat. *J Bone Joint Surg*, vol 45A, pp. 35-44, 1963.
- [12] Wilson PD. Capsulectomy for the relief of flexion contractures of the elbow following fracture. *J Bone Joint Surg*, vol 26A, pp. 71-86, 1944.

- [13] Wagner LC. Fixed extension of the knee due to capsular contraction. NY State J Med, vol 48, pp. 194-198, 1948.
- [14] Trudel G, Desaulniers N, Uthoff HK, Laneuville O. Different levels of COX-1 and COX-2 enzymes in synoviocytes and chondrocytes during joint contracture formation. J Rheumatol, vol 28, pp. 2066-2974, 2001.
- [15] Trudel G, Uthoff HK, Brown M. Extent and direction of joint motion limitation after prolonged immobility: an experimental study in the rat. Arch Phys Med Rehabil, vol 80, pp. 1542-1547, 1999.
- [16] Finsterbush A, Friedman B. Early changes in immobilized rabbit knee joints: a light and electron microscopic study. Clin Orthop, vol 92, pp. 305-319, 1973.
- [17] Roy S. Ultrastructure of articular cartilage in experimental immobilization. Ann Rheum Dis, vol 29, pp. 634-642, 1970.
- [18] Woo SL, Matthews JV, Akenon WH, Amiel D, Convery FR. Connective tissue response to immobility: Correlative study of biomechanical measurements of normal and immobilized rabbit knees. Arthritis Rheum, vol 18, pp. 257-264, 1975.
- [19] Hozumi N, Yamashita R, Lee CK, Nagao M, Kobayashi K, Saijo Y, Tanaka M, Tanaka N, Ohtsuki S. Time-frequency analysis driven ultrasonic microscopy for biological tissue characterization. Ultrasonics, vol 42, pp. 717-722, 2004.
- [20] Saijo Y, Tanaka M, Okawai H, Sasaki H, Nitta S, Dunn F. Ultrasonic tissue characterization of infarcted myocardium by scanning acoustic microscopy. Ultrasound Med Biol, vol 23, pp. 77-85, 1997.
- [21] Saijo Y, Sasaki H, Okawai H, Nitta S, Tanaka M. Acoustic properties of atherosclerosis of human aorta obtained with high-frequency ultrasound. Ultrasound Med Biol, vol 24, pp. 1061-1064, 1998.
- [22] Saijo Y, Jorgensen S, Mondek P, Sefranek V, Paaske W. Acoustic inhomogeneity of carotid arterial plaques determined by GHz frequency range microscopy. Ultrasound Med Biol, vol 28, pp. 933-977, 2002.
- [23] Shollmeier G, Sarkar K, Fukuhara K, Uthoff HK. Structural and functional changes in the canine shoulder after cessation of immobilization. Clin Orthop, vol 323, pp. 310-315, 1996.

The High-frequency Acoustic Properties of the Rabbit Supraspinatus Tendon Insertion

A comparison between decalcified and undecalcified specimens

Hiroataka Sano, MD[†], Koshi Hattori, MD[†], Yoshifumi Saijo, MD[‡]
and Shoichi Kokubun, MD[†]

[†]Department of Orthopaedic Surgery, Tohoku University, School of Medicine

[‡]Department of Medical Engineering and Cardiology, Institute of Development, Aging and Cancer, Tohoku University
Sendai, Japan

E-mail: staka@mail.tains.tohoku.ac.jp

Abstract— To clarify whether decalcification altered the tissue high-frequency acoustic properties or not, supraspinatus tendon insertion of 6 Japanese white rabbits were measured with scanning acoustic microscopy. Right supraspinatus tendons attached to the humeral head were cut into two pieces at the center of the tendon. Then, they were fixed with 10% neutralized formalin for 12 hours. In each specimen, medial half was not decalcified, while lateral half was decalcified with ethylene-diamine-tetra-acetic acid. After embedding in paraffin, they were cut at a thickness of 5 μ m for the measurement with scanning acoustic microscopy. The sound speed in each histologic zone was evaluated, which were then compared between the undecalcified and the decalcified specimens.

Mean sound speed of non-mineralized fibrocartilage was 1575m/s in the undecalcified specimens and 1572m/s in the decalcified specimens. On the other hand, it decreased 3-5% after decalcification in the mineralized tissue including mineralized fibrocartilage and bone (mineralized fibrocartilage: undecalcified = 1756m/s, decalcified = 1672m/s; bone: undecalcified = 1800m/s, decalcified = 1746m/s). However, no statistically significant differences were found between the undecalcified and the decalcified specimens. We believe that the scanning acoustic microscopy can be applied for the specimens including mineralized tissue after decalcification.

Keywords—Scanning acoustic microscopy, sound speed, supraspinatus tendon, insertion, decalcification

I. INTRODUCTION

Scanning acoustic microscopy (SAM) has been used to assess the high-frequency acoustic

properties of various types of soft tissue, representing complex histologic structures, i.e. cardiac muscles, arterial plaques and vascular walls, etc [1-3]. One of the major advantages of SAM is that tissue elasticity can be measured with formalin-fixed and paraffin-embedded glass slides. This makes it possible to compare the 2-dimensional distribution of the tissue elasticity to the histologic structure. Since, however, the role of decalcification has not been investigated yet in SAM measurement, we attempted to clarify the roles of decalcification in SAM measurement in the current study. Especially, we hoped to know whether decalcification alter the tissue high-frequency acoustic properties of the non-mineralized fibrocartilage at the insertion of the rabbit supraspinatus tendon or not.

II. MATERIALS AND METHODS

A. Preparation of the specimens

Supraspinatus tendon insertions of 6 Japanese white rabbits were used for the current study. All these animals were 12 month-old males and their average body weight was 2.3kg (range: 2.2-2.4kg). After euthanasia with overdosed pentobarbital, right supraspinatus tendons attached to the humeral head were collected. The specimens were cut into two pieces at the center of supraspinatus tendon in line with its fibers and bony tissue was carefully removed except for the insertion site. Then, they were fixed with 10% neutralized formalin for 12 hours.

In each animal, medial half of the specimen was not decalcified, while lateral half of the specimen was decalcified with ethylene-diamine-tetra-acetic acid (EDTA). After embedding in paraffin, they were cut at a thickness of 5 μ m both for the histologic staining and for the measurement with SAM.

B. Histologic staining

Haematoxylin-eosin (HE) staining was routinely employed to assess the overall histologic structure. Both the area of non-mineralized fibrocartilage and that of the mineralized fibrocartilage were determined histologically. Photographs were taken under the microscope, which were trimmed thereafter to create histologic images with areas identical to those of the SAM measurements.

C. SAM measurement

A specially developed SAM system in Tohoku University, operating in the frequency range of 100-200MHz, was used for this study. Distilled water was used as the coupling medium, which maintained the specimen at 20°C during the measurement procedure.

The sections for SAM measurements were mounted on glass slides but not covered by cover slips. The paraffin was removed from the sections by the graded alcohol method prior to the ultrasonic measurement. Since the fibrocartilage was the most distinct in the deep part of the tendon insertion, we determined to focus on the articular half of the insertion site [4]. The data of the sound speed obtained were converted into color signals on the computer. Two-dimensional distribution pattern of the sound speed was displayed and saved as an image file using a color-coded scale.

D. Data interpretation

The value of the sound speed was evaluated in each histologic zone. The most predominant two color-codes were chosen and recorded for each zone, which were then compared between undecalcified and decalcified specimens. For statistical analyses, the average value of the sound speed was established in each zone. Paired t-test was used for determining the statistical differences between undecalcified and decalcified specimens.

III. RESULTS

The 2-dimensional distribution of sound speed indicated almost identical pattern between undecalcified and decalcified specimens (Fig. 1-a,b, 2-a,b). Non-mineralized fibrocartilage represented the lowest value in sound speed among 4 zones of the supraspinatus tendon insertion. Mean sound speed of this zone was 1575m/s in undecalcified specimens and 1572m/s in decalcified specimens.

In the mineralized tissue (mineralized fibrocartilage and bone), sound speed decreased 3-5% after decalcification. The mean sound speed of mineralized fibrocartilage was 1756m/s in the

undecalcified specimens and 1672m/s in the decalcified specimens. In bone, it was 1800m/s in the undecalcified specimens and 1746m/s in the decalcified specimens (Fig. 2). However, no significant differences were found statistically between the undecalcified and the decalcified specimens.

IV. DISCUSSION

In SAM measurements, the preparation of specimens including formalin fixation, dehydration and paraffin embedding might alter the tissue high-frequency acoustic properties. In 1996, Sasaki et al. confirmed that such tissue preparations did not change the high-frequency acoustic properties of the normal kidney tissue significantly [5]. Their study clearly indicated that the relative relationships of the high-frequency acoustic properties was well preserved after these preparation process. Unfortunately, however, the roles of decalcification in SAM measurement have not been clarified yet. Thus, the application of this technology to the Orthopaedic field has been very limited.

Previous authors mainly used undecalcified specimens embedded in methylmethacrylate for SAM measurement [6-8]. However, there are several disadvantages to use these undecalcified specimens. First, preparation of sections including the process of grinding and polishing is very time consuming. Second, it is technically difficult to control the thickness of the sections constant during such preparation process. If the thickness of tissue is uneven among specimens, it might cause some errors during SAM measurement. Third, it is rather difficult to perform histologic investigations with such grinded undecalcified sections. Especially for immunohistochemical staining, most antibodies have been developed for formalin-fixed and paraffin-embedded specimens. All these disadvantages make it difficult to compare the tissue high-frequency acoustic properties to the histologic or immunohistochemical characteristics. Therefore, we believe that it is much more convenient to use the decalcified specimens than to use the undecalcified specimens for SAM measurement.

The results of the current study revealed that the high-frequency acoustic properties in soft tissues including non-mineralized fibrocartilage were not altered significantly by decalcification. On the other hand, the sound speed decreased 3-5% after decalcification in the mineralized tissue including mineralized fibrocartilage and bone. However, there were no statistically significant differences between

the undecalcified and the decalcified specimens. Based on these findings, we conclude that the sound speed measured with SAM is not altered significantly with EDTA decalcification. We believe that SAM can be used more widely even for specimens including mineralized tissue.

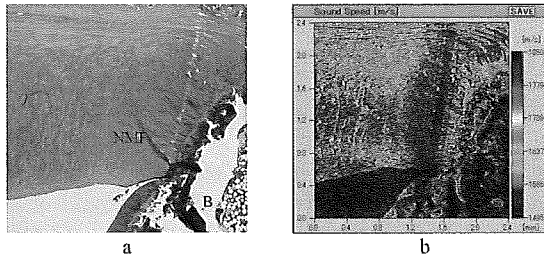


Figure 1: Sound speed in undecalcified specimen (Rabbit No.6).

a: haematoxylin-eosin, b: sound speed

Non-mineralized fibrocartilage is depicted with blue and black. On the other hand, mineralized fibrocartilage and bone were depicted with green and red (NMF: non-mineralized fibrocartilage, B:bone).

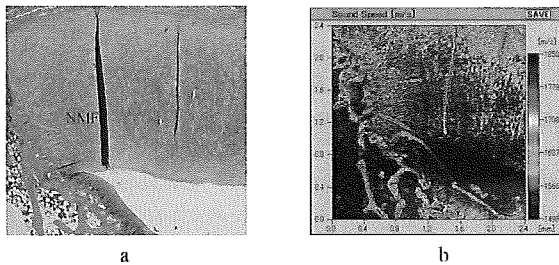


Figure 2: Sound speed in decalcified specimen (Rabbit No.6).

a: haematoxylin-eosin, b: sound speed

In decalcified specimens, non-mineralized fibrocartilage is also depicted with blue and black. In mineralized tissue, both mineralized fibrocartilage and bone are depicted with green and yellow (NMF: non-mineralized fibrocartilage, B:bone).

REFERENCES

- [1] Y. Saijo, M. Tanaka, H. Okawai, H. Sasaki, S-I. Nitta, F. Dunn, Ultrasonic tissue characterization of infarcted myocardium by scanning acoustic microscopy. *Ultrasound Med. Biol.* 23(1) (1997) 77-85.
- [2] Y. Saijo, H. Sasaki, H. Okawai, S-I. Nitta, M. Tanaka, Acoustic properties of atherosclerosis of human aorta obtained with high-frequency ultrasound. *Ultrasound Med. Biol.* 24(7)(1998) 1061-1064.
- [3] Y. Saijo, C.S. Jørgensen, E. Falk, Ultrasonic tissue characterization of collagen in lipid-rich plaques in apoE-deficient mice. *Atherosclerosis* 158 (2001) 289-295.
- [4] M. Benjamin, J.R. Ralphs, Fibrocartilage in tendons and ligament-an adaptation to compressive load. *J Anat* 193 (Pt 4) (1998) 481-494.
- [5] H. Sasaki, Y. Saijo, M. Tanaka, H. Okawai, Y. Terasawa, T. Yambe, Nitta S-I, Influence of tissue preparation on the high-frequency acoustic properties of normal kidney tissue. *Ultrasound Med Biol* 22(9) (1996) 1261-1265.
- [6] K. Hasegawa, C.H. Turner, R.R. Recker, E. Wu, D.B. Burr, Elastic properties of osteoporotic bone measured by scanning acoustic microscopy. *Bone* 16(1) (1995) 85-90.
- [7] C.H. Turner, J. Rho, Y. Takano, T.Y. Tsui, G.M. Pharr, The elastic properties of trabecular and cortical bone tissues are similar: results from two microscopic measurement techniques. *J Biomechanics* 32 (1999) 437-441.
- [8] T. Nomura, E. Gold, M.P. Powers, S. Shingaki, J.L. Katz, Micromechanics/structure relationship in the human mandible. *Dental Materials* 19 (2003) 163-173.

- [1] Y. Saijo, M. Tanaka, H. Okawai, H. Sasaki, S-I. Nitta, F. Dunn, Ultrasonic tissue characterization